



Supporting Information

Eco-friendly Self-Powered X-ray Detector Based on a Multi-layered Double Perovskite Ferroelectric

Qi Gao^{a†}, Kuanhai Li^{a†}, Yingying Zheng^a, Panpan Yu^{*a,b}, Yunpeng Yao^c, Zeng-Kui Zhu^a, and Junhua Luo^{*a,b}

^a Jiangxi Normal University, School of Chemical Engineering, Nanchang, Jiangxi 330022, China

^{*}Junhua Luo, E-mail: luojunhua@jxnu.edu.cn; Panpan Yu, Email: ppyu@jxnu.edu.cn

^b Fujian Institute of Research on the Structure of Matter, Chinese Academy of Sciences, State Key Laboratory of Structural Chemistry, Fuzhou, Fujian 350002, China

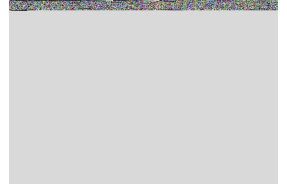
^c Yantai University, School of Environmental and Material Engineering, Yantai 264005, P. R. China

[†] Q. G., and K. L. contributed equally to this work

Experimental Section

Synthesis and crystal growth: benzylamine (BZA, Aladdin, 99%), Ag₂O (Aladdin, 99.7%), Bi₂O₃ (Aladdin, 99.9%), hydriodic acid solution (HI, Aladdin, 48 wt.%), Cs₂CO₃ (98%) were purchased and used without further purification. The Ag₂O, Bi₂O₃, benzylamine and Cs₂CO₃ were dissolved in aqueous HBr solution (20 mL, 48%) with molar ratio of 1:1:2:1 to form a yellow solution. Subsequently, the yellow single crystals were grown from saturated solution *via* temperature lowering method in the range from 70 to 30 °C with cooling rate of 1 K per day. Finally, the high-quality crystals could be gained after several days.

Physical properties measurements: The PXRD were collected in the in the 2θ range of 5 ~ 50° with a step size of 0.05° on the MiniFlex 600 X-ray diffractometer with a CuKα source (λ = 1.541 Å). Thermogravimetric analysis (TGA) was performed on STA449C Thermal Analyser ranging from the room temperature to 1000 K. The Differential scanning calorimetry (DSC) was conducted on a NETZSCH DSC 200F3 DSC instrument in range from 370 to 440 K with a heating/cooling rate of 10 K min⁻¹ under N₂ atmosphere.



X-ray detection measurements: The I - V and I - t curves were conducted using a high precision electrometer (Keithley 6517B). The X-ray source was an Amptek Mini-X2 X-ray tube with silver target (maximum power 4 W) with the maximum X-ray photons energy of 50 keV. The dose rate was measured by a Radcal Accu-Gold X-ray dosimeter attached with the 10×6-180 ion chamber in an integrating mode and it can be changed by its tube current. The sensitivity (S) is defined as the collected charge per unit under the X-ray irradiation and can be determined by the following equation:

$$S = \frac{I_p - I_d}{D \times A}$$

where I_p is the photocurrent under X-ray irradiation, I_d is the dark current, D is the dose rate and A is the device area.

signal-to-noise (SNR) can be calculated by the following equation:

$$SNR = \frac{I_{\text{signal}}}{I_{\text{noise}}} = \frac{I_p - I_d}{\sqrt{\frac{\sum_{i=1}^n (I_i - I_p)^2}{n}}}$$

where I_{signal} is the signal current and I_{noise} is the signal current, I_p is the average current under X-ray irradiation, I_d is the average dark current.

The temperature during X-ray detection measurements was controlled using a Linkam TS1500 heating stage.

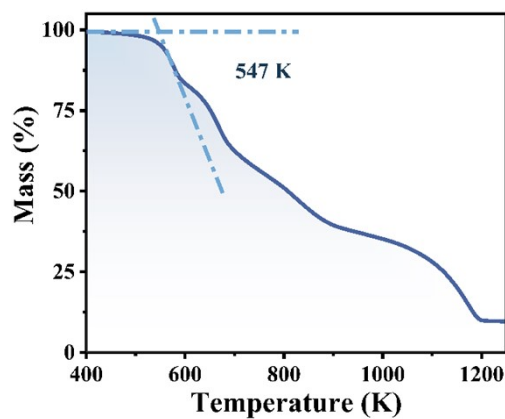


Figure S1. TG curve of 1.

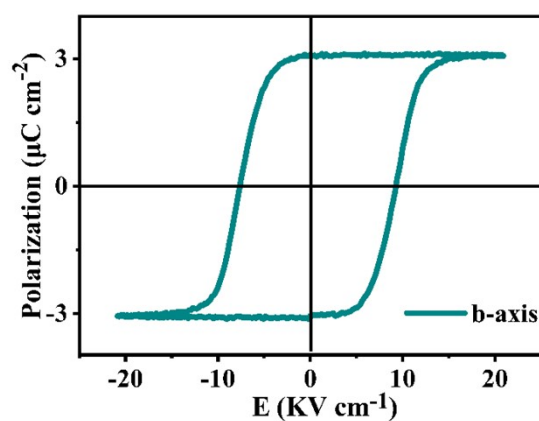


Figure S2. Ferroelectric hysteresis loop of **1** at 350 K.

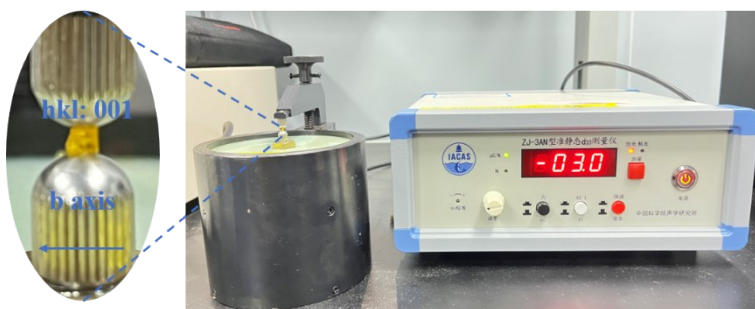


Figure S3. The piezoelectric performance of Compound **1**.

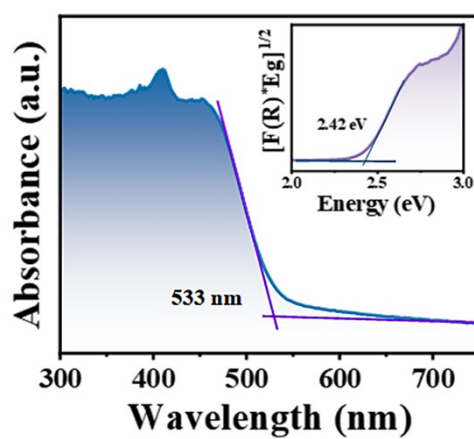


Figure S4. The absorption spectrum and estimated bandgap (inset) of **1**.

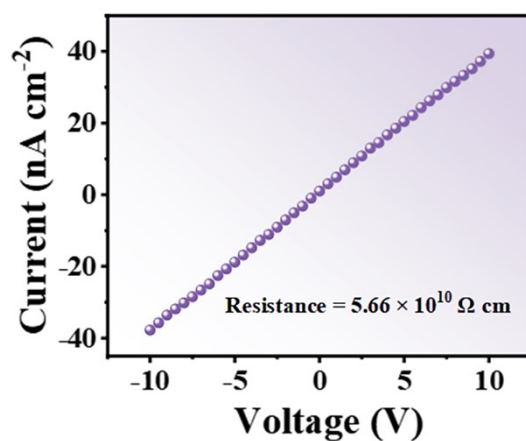


Figure S5. Resistivity of **1** SC along the b-axis.

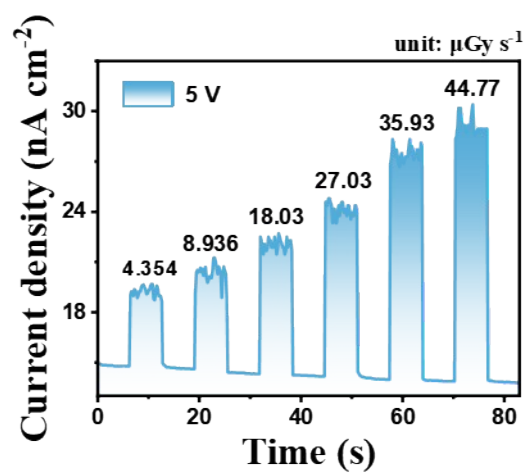


Figure S6. Current density-time curves of **1** SC detector at 25 °C under increased X-ray dose rates at 5 V.

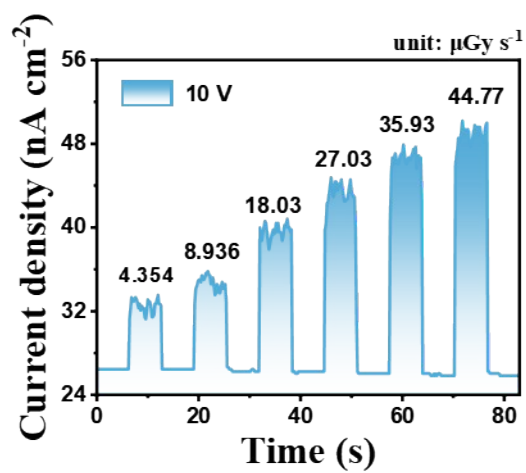


Figure S7. Current density-time curves of **1** SC detector at 25 °C under increased X-ray dose rates at 10 V.

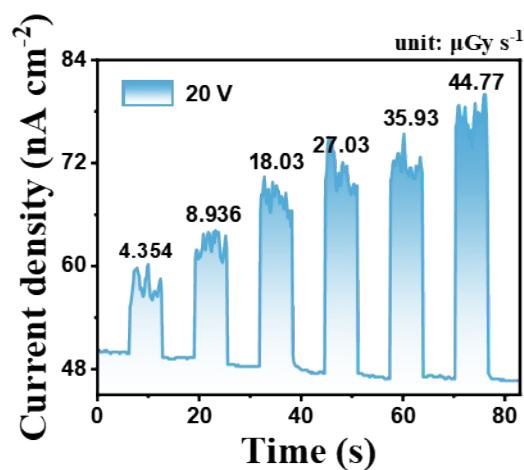


Figure S8. Current density-time curves of **1** SC detector at 25 °C under increased X-ray dose rates at 20 V.

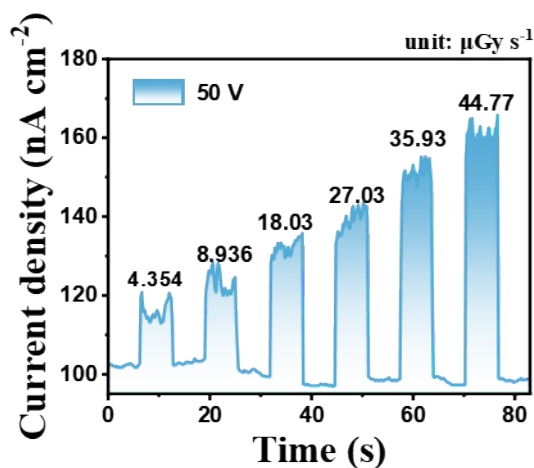


Figure S9. Current density-time curves of **1** SC detector at 25 °C under increased X-ray dose rates at 50 V.

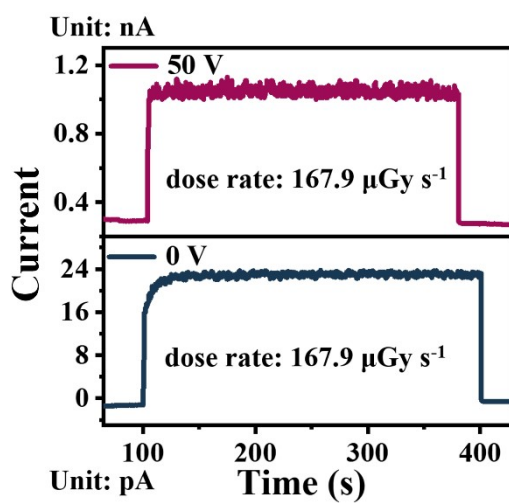



Figure S10. Radiation stability of **1** device.

Table S1. Performance comparison of the 1 SC detector and some reported HDP X-ray detectors.

Dimensionally	Compound	Sensitivity ($\mu\text{C Gy}^{-1} \text{ cm}^{-2}$)	Detection limit (nGy s^{-1})	Refs.
2D	$\text{BA}_4\text{AgBiBr}_8$	1876 (-)	34.3 (200 V)	[1]
2D	$(\text{PA})_4\text{AgBiBr}_8$	1243 (-)	145.1 (200 V)	[1]
2D	$\text{BDA}_2\text{AgBiBr}_8$	2638 (200 V)	7.4 (200 V)	[1]
3D	$\text{Cs}_2\text{AgBiBr}_6$	105 (50 V)	59.7 (5 V)	[2]
0D	$\text{FA}_3\text{Bi}_2\text{I}_9$	598.1 (500 V)	0.2 (180 V)	[3]
3D	$\text{PEA-Cs}_2\text{AgBiBr}_6$	288.8 (50 V)	-	[4]
2D	$(4\text{-AP})_2\text{AgBiBr}_8$	1117.3 (80 V)	279 (10 V)	[5]
2D	$(\text{BrPA})_4\text{AgBiBr}_8$	517 (40 V)	-	[6]
2D	$(4,4\text{-DFPD})_4\text{AgBiI}_8$	188 (50 V)	3130 (50 V)	[7]
2D	$(\text{HIA})_2\text{AgBiBr}_8$	118 (10 V)	4300 (10 V)	[8]
2D	$(\text{FPEA})_4\text{AgBiBr}_8$	27 (333 V mm^{-1})	2600 (333 V mm^{-1})	[9]
2D	$(\text{I-BA})_4\text{AgBiI}_8$	5.38 (10 V)	-	[10]
2D	$(\text{C}_6\text{H}_5\text{CH}_2\text{NH}_3)_2\text{CsAgBiBr}_7$	1154.8 (50 V)	716 (0 V)	This work

Reference

- [1] H. Chen, Z. Li, S. Wang, G. Peng, W. Lan, H. Wang, Z. Jin, Molecular Design of Layered Hybrid Silver Bismuth Bromine Single Crystal for Ultra-Stable X-Ray Detection With Record Sensitivity. *Adv. Mater.* **2024**, *36*, 2308872.
- [2] Y. Xu, J. Hu, X. Xiao, H. He, G. Tong, J. Chen, Y. He, Evaporation crystallization of zero-dimensional guanidinium bismuth iodide perovskite single crystal for X-ray detection. *Inorg. Chem. Front.* **2022**, *9*, 494.
- [3] W. Li, D. Xin, S. Tie, J. Ren, S. Dong, L. Lei, X. Zheng, Y. Zhao, W. Zhang, Zero-Dimensional Lead-Free $\text{FA}_3\text{Bi}_2\text{I}_9$ Single Crystals for High-Performance X-ray Detection. *J. Phys. Chem. Lett.* **2021**, *12*, 1778–1785.
- [4] W. Yuan, G. Niu, Y. Xian, H. Wu, H. Wang, H. Yin, P. Liu, W. Li, J. Fan, In Situ Regulating the Order–Disorder Phase Transition in $\text{Cs}_2\text{AgBiBr}_6$ Single Crystal toward the Application in an X-Ray Detector. *Adv. Funct. Mater.* **2019**, *29*, 1900234.
- [5] G. Chen, H. Dai, Z.-K. Zhu, J. Wu, P. Yu, Y. Zeng, Y. Zheng, L. Xu, J. Luo, Dion-Jacobson Type Lead-Free Double Perovskite with Ultra-Narrow Aromatic Interlayer Spacing for Highly Sensitive and Stable X-ray Detection. *Small* **2024**, *20*, 2312281.
- [6] Z. Yue, F. Wu, X. Li, Y. Liu, J. Luo, X. Liu, Centimeter-sized single crystal of a lead-free halide double perovskite with ferroelastic phase transition-triggered switchable dielectric properties. *Sci. China-Mater.* **2023**, *66*, 3977.
- [7] C.-F. Wang, H. Li, M.-G. Li, Y. Cui, X. Song, Q.-W. Wang, J.-Y. Jiang, M.-M. Hua, Q. Xu, K. Zhao, H.-Y. Ye, Y. Zhang, Centimeter-Sized Single Crystals of Two-Dimensional Hybrid Iodide Double Perovskite $(4,4\text{-Difluoropiperidinium})_4\text{AgBiI}_8$ for High-Temperature Ferroelectricity and Efficient X-Ray Detection. *Adv. Funct. Mater.* **2021**, *31*, 2009457.
- [8] W. Guo, H. Xu, Q. Fan, P. Zhu, Y. Ma, Y. Liu, X. Zeng, J. Luo, Z. Sun, Centimeter-Size Single Crystal of a Polar Dion–Jacobson Double Perovskite with Large Mobility-Lifetime Product toward Effective X-Ray Detection. *Adv. Optical Mater.* **2024**, *12*, 2303291.
- [9] M. Ge, S. Chen, X. Fu, Y. Feng, D. Wang, M. Yuan, Effects of fluorinated aromatic spacer in Ag–Bi double perovskite for X-ray detector. *J. Phys. Chem. C* **2022**, *126*, 19417.

- 
- [10] Z. Xu, H. Wu, D. Li, W. Wu, L. Li, J. Luo, A lead-free I-based hybrid double perovskite (I-C₄H₈NH₃)₄AgBiI₈ for X-ray detection. *J. Mater. Chem. C* **2021**, 9, 13157.